JOURNAL OF MATERIALS SCIENCE 25 (1990) 4949–4956

Fracture analysis of cobalt-bonded tungsten carbide composites

D. HAN*, J. J. MECHOLSKY, Jr.‡
Department of Materials Science and Engineering, The Pennsylvania State University, University Park, Pennsylvania 16802, USA

Specimens of WC–Co were indented to measure the resulting crack size and unindented samples were fractured in three-point flexure to obtain strength and to measure characteristic features on the fracture surface. Fracture toughness was determined using indentation techniques and compared to those determined using fractography. We show that principles of fracture mechanics can be applied to WC–Co composites and can be used to analyse the fracture process.

The fracture surfaces were examined by scanning electron microscopy and optical microscopy. Characteristic features observed in glasses, single crystals and polycrystalline materials known as mirror, mist, hackle and crack branching were identified for these composites. We discuss the importance of fracture surface analysis in determining the fracture origins and in the failure analysis of WC–Co composites.

1. Introduction

Cobalt-bonded WC composites show high fracture toughness, hardness and strength compared to other ceramic materials. All of these properties make the composites attractive for use in challenging environments like those in metal cutting, drilling and tool inserts. As a consequence, great attention has been paid to the evaluation of mechanical properties [1–3]. Much literature is devoted to the study of strength of these materials [3]. In addition, in more recent years attention has been devoted to the fracture toughness of WC–Co, i.e., the critical strength intensity factor [4–6]. There appears, however, to be some discussion over the proper test to use in measuring the toughness [7, 8]. Single-edge notched beam (SENB) [5, 6, 9], chevron-notched beam (CNB) [10], double cantilever beam (DCB) [11–13] and indentation crack tests [14–19] have all been used on these materials to measure the resistance to fracture. These tests do not always provide similar estimates of the value for fracture toughness. It is understandable if the SENB, CNB and DCB tests give different values to the indentation type tests because the indentation tests use smaller cracks than any of the other tests and small cracks can behave differently to large cracks [20]. The greatest controversy occurs with the small cracks associated with the indentation technique [10–13]. Discussion of whether or not Palmqvist type cracks occur and what specific equation should be used, if indeed they do occur, has generally been at the focus of the controversies for not only these materials but other ceramics as well [7]. Most failures in ceramics including WC–Co, however, occur from cracks or defects of the size of indentation cracks [5], so it is important to understand their behaviour.

This paper addresses the analysis of fracture by indentation cracking to determine the most appropriate existing expression for determining the resistance to fracture as measured by fracture toughness. The results are confirmed by fracture surface analysis where the critical cracks that cause failure and the surrounding topography are observed. We determined that the indentation techniques of Lawn, Marshall and coworkers [18, 19] agree with the large crack techniques for two cobalt content tungsten carbide composites.

2. Background

2.1. Failure mechanisms of WC–Co

The failure behaviour of WC–Co cermets has been investigated for several decades [1, 4–7, 11–13, 21]. For instance, it is reported that, like other brittle materials, larger WC particles, i.e., grains, fracture transgranularly and smaller particles fracture intergranularly [21]. Also there are generally four failure modes for WC–Co composites [5, 21]. (1) The first is fracture of WC particles in which multiple interfacial decoherence of WC particles leaves a pattern of ruptured cobalt ligaments on the larger WC particle face at one fracture surface, and leaves several smooth WC particles surrounded by a cobalt ridge on the opposite fracture surface. (2) The second is brittle fracture of WC–WC boundaries which includes transgranular or intergranular microcracking of WC particles; the broken or debonded particles are surrounded by a coarse ridge of cobalt binder phase which matches on

*Present address: RIST, Ceramics Materials Division, P.O. Box 135, Pohang, South Korea.
‡Present address: Department of Materials Science and Engineering, University of Florida, Gainesville, FL 32611, USA.

0022–2461/90 $03.00 + .12

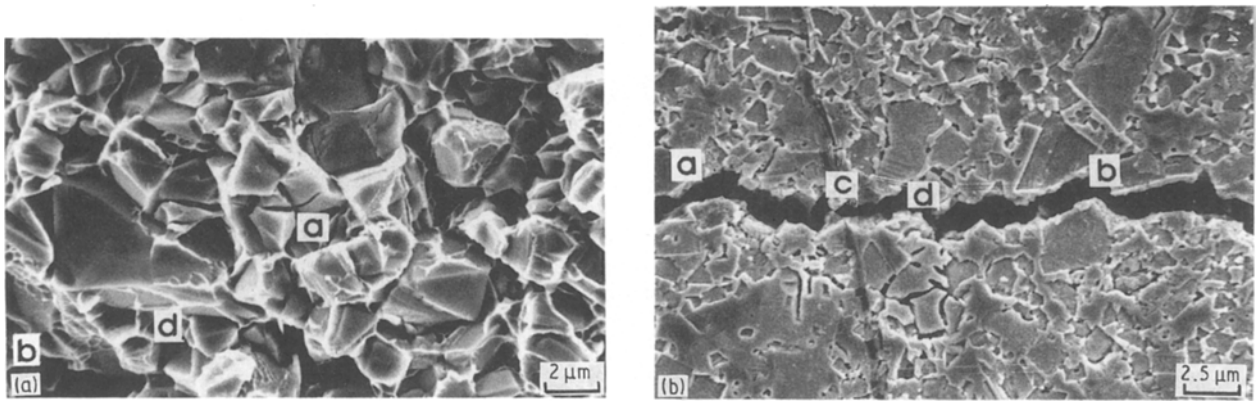

Figure 1 Observation of (a) fracture surface and (b) chemically etched surface illustrating fracture modes in WC–Co composite. Cracks were produced by Vickers indentation technique used in this study. (a, fracture of WC particles; b, interfacial decoherence of WC particles; c, fracture of cobalt phase; d, separation of WC–Co interface).

both fracture surfaces. If the separation takes place by WC–WC interfacial decohesion, the particle shapes will be different on the other side. (3) The third is ductile tearing of the cobalt phase where the rupture of the cobalt layer of non-uniform thickness leaves a pattern of dimples or tear ridges on both fracture surfaces. In general, the thinner the cobalt layer, the smaller the size of dimples. (4) The fourth is decoherence of WC–Co interfacial boundaries where the WC–Co interface failure after appreciable deformation leaves the WC and cobalt phase with a pattern of tearing ridges. The fracture of WC grains and cobalt binder phase are the most common failure modes. These are easily seen by optical microscopy or scanning electron microscopy (SEM) using indentation techniques (Fig. 1). Fracture of WC–WC grain boundaries usually take place first and the rupture of the cobalt binder region follows.

2.2. Indentation techniques

Previous failure analyses and toughness measurements were mostly limited to surface microcracking and low indentation loads (< 1000 N). In addition to these observations by surface indentation it is recommended that the fracture surfaces of unindented and indented specimens are examined in order to understand better how WC–Co composites fail and to determine proper analyses for fracture toughness. Shetty and coworkers [7] reported that fracture in WC–Co cermets obeys the Palmqvist crack model because cracks emanating from the ends of the indenter follow a linear dependence of crack dimensions on indentation loads rather than the 3/2 powder dependence expected for the radial–median crack model.

They observed the Palmqvist cracks in cemented carbides by sequential polishing [7] of the indentation impression area while monitoring surface removal. Lankford [8] indicated that the half-penny crack model is observable at higher indentation loads, thus, there is still some question whether WC–Co fits the Palmqvist crack or half-penny crack models, or both.

The equation for fracture toughness by indentation for WC–Co composites based on the Palmqvist crack model [7, 22] is as follows

$$K_C = 0.089(HW)^{1/2} \quad (1)$$

where H is hardness, W a crack resistance parameter [22, 23] which can be obtained from $W = (P - P_0)/4a$ or $W = P/4a$, where P is the indentation load and P_0 is an experimentally determined threshold indentation load for cracking, and a is the mean Palmqvist crack length (Fig. 2).

Anstis *et al.* [18, 19] have shown that for many materials, a Vickers or Knoop indentation can produce a model flaw with which to study the fracture process. The cracks resulting from residual contact stresses during and after the indentation process can be used to estimate the fracture toughness using a measurement of the crack size from the surface trace (Equation 2):

$$K_C = 0.016(E/H)^{1/2}Pc^{-3/2} \quad (2)$$

where E is the elastic modulus and c the crack length as shown in Fig. 2.

2.3. Fracture surface analysis

Observations of the fracture surfaces of fractured specimens provide much information about the failure source, fracture process and fracture toughness evaluation. Most fracture surfaces can be examined by optical or scanning electron microscopy. Fig. 3 represents a schematic of the different features observed in

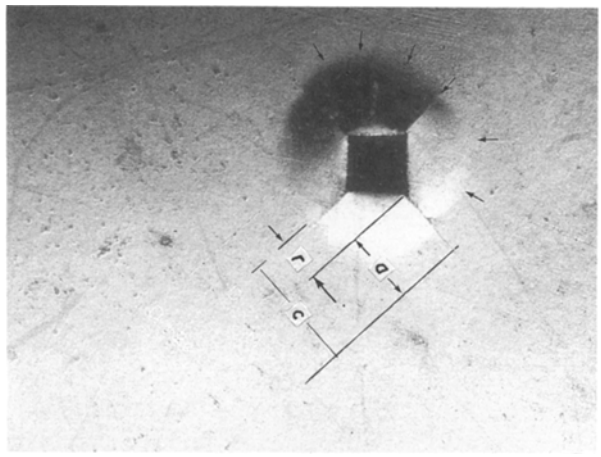

Figure 2 Optical micrograph demonstrating the Vickers indentation and associated parameters. The shaded and light region outlined by the arrows shows a region of lateral, subsurface cracks due to the indentation process. a is the Palmqvist crack length, r the half diagonal of impression and c the crack length $(a + r)$.

glass, single crystals and polycrystalline materials known as the failure initiating flaw, the mirror, mist and hackle regions, and crack branching [24]. In fine grain materials failing intergranularly and in larger grain materials failing transgranularly [19], failure sources generally can be easily identified and measured. Without the presence of residual stress, fracture toughness can be estimated from fractography [25–27] using Equations 3 and 4:

$$K_C = 1.24\sigma_f C^{*1/2} \quad (3)$$

where C^* is the flaw size determined by $C^* = (a^*b^*)^{1/2}$, where a^* is the semi-minor axis, b^* the semi-major axis of an elliptical flaw and σ_f is the applied stress at failure

$$K_C = 1.24M_i(C^*/R_i)^{1/2} \quad i = 1, 2, 3 \quad (4)$$

where M_i is the corresponding mirror constant obtained by $M_i = \sigma_f R_i^{1/2}$; $i = 1, 2, 3$ corresponds to the mirror–mist, mist–hackle and macroscopic crack branching boundaries, respectively. It should be noted that the measurements of R_i must be made along the tensile surface to use Equation 4. It has been shown that these mirror constants are generally independent of the rate and type of loading [25, 26].

More recently, Kirchner and Conway [28–30] showed that the stress intensity approach of Newman and Raju [31] developed for surface cracks, could be applied to the fracture mirror boundaries, thus, for each boundary there is a critical value of the branching constant, K_{Bi}. These values are valid for all measurements of R_i along the crack periphery. It can, however, be shown that for most cases K_{Bi} is directly related to M_i at the surface [28, 32]. Thus, it can be shown that

$$K_{Bi} = 1.24M_i \quad i = 1, 2, 3 \quad (5)$$

where K_{Bi} is branching stress intensity factor.

3. Experimental procedures

10 and 16 wt % cobalt-bonded tungsten carbide composites were indented with a Vickers diamond. Residual stress due to grinding of WC–Co composites can influence the measurement of toughness and strength [7], therefore, before indentation, to remove the grinding zones on the surface, three sequential steps of polishing were required: 3 min with a 15 μm, 10 min with a 6 μm and 10 min with a 1 μm diamond compound using an automatic polisher. After polishing all of the indentations were performed with a Vickers hardness indenter on a compressive testing machine* using loads between 500 and 2500 N. The loading rates were 0.0008 mm sec^{-1} under 1000 N and 0.0004 mm sec^{-1} for up to 2500 N to avoid indenter damage and any impact effect; the load was held for 15 sec and released at the same speed as that of the loading. The average crack sizes and hardness impressions were determined by optical microscopy. Also, unindented specimens (as-received) of these composites were fractured in three-point bending for strength measurements and fracture surface analysis.

*Instron Engineering Corporation, Canton, Massachusetts.

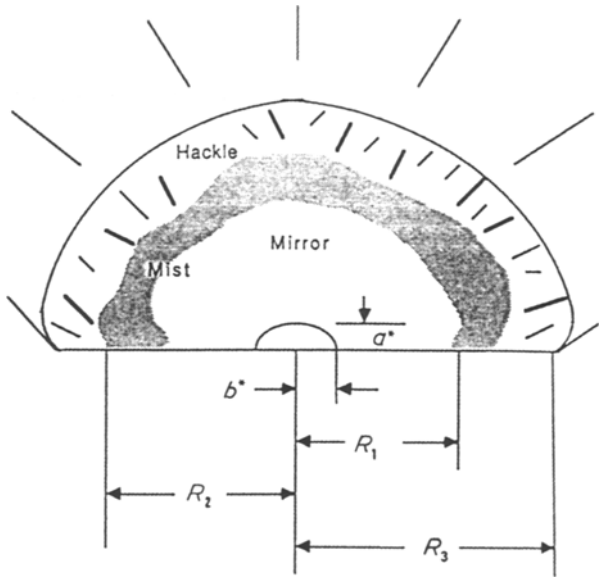

Figure 3 A schematic of the fracture surface including mirror, mist and hackle regions, and macroscopic crack branching. C^* is the size of failure-initiating crack ($=(a^*b^*)^{1/2}$), R_1 the mirror–mist boundary, R_2 the mist–hackle boundary and R_3 the hackle–crack branching boundary.

The microstructures of 10 and 16 wt % cobalt-bonded WC composites were examined after chemical etching; this includes the immersion of polished bars in a chemical solution (10 ml water + 1 g KOH + 1 g $K_3Fe(CN)_6$) for 3 to 5 min. The samples were flushed with water and cleaned using a sonic resonance cleaner for about 30 min.

Fracture surfaces were examined optically, and the features (Fig. 3) were measured with a microscope. Flaw and mirror sizes were always measured along the tensile surface. For an asymmetric feature of mirror boundary the longer R_i was used for property evaluation [26].

4. Results and discussion

The chemically etched microstructures of WC with different cobalt content are shown in Fig. 4. Measurements of crack size and surrounding topography are presented in Table I. Table II shows the values of strength, hardness and fracture toughness of 10 and 16 wt % cobalt-bonded WC cermets calculated using indentation techniques, fracture surface analysis and the data in Table I. Fracture toughness values based on $W = (P - P_0)/4a$ (Palmqvist crack model) are relatively high for WC–Co compared to large crack data [6, 9–13]. If the classical Palmqvist crack model is used, i.e. with $P_0 = 0$, then the values would be even higher and unrealistic. This shows that the Palmqvist crack model is not appropriate for these WC–Co composites regardless of the indentation load. If the presumed half-penny crack length (c) is used in place of a in Equation 1 with $P_0 = 0$, then reasonable values are obtained for the toughness of WC–Co. This agreement may be fortuitous or may have significance. Even though there is no justification for $W = P/4c$, fracture toughness based on $W = P/4c$ seems to be acceptable.

TABLE I Observed data† from fracture surface analysis of WC–Co composites

Sample	a^*	$2b^*$	C^* (μm)	R_1	R_2	R_3	σ_f (MPa)
10Co-a[a]	50	133	58	330	700	1050	1548
10Co-b	50	70	42	233	500	733	1901
10Co-c[b]			58	333	500	900	1753
10Co-d	45	133	55	300	600	1000	1647
10Co-e[a]	33	100	41	200	400	600	2053
10Co-f[a]	33	100	41	175	430	630	2084
10Co-g[c]	50	65	40	165	400	600	2273
10Co-h	45	65	38	200	350	600	2200
10Co-i[b]			34	230	465	660	1897
10Co-j	45	65	38	200	400	730	2043
10Co-k[b]			325	560	1000	1500	772
10Co-l[a]	45	133	55	250	530	750	1958
10Co-m[b]			45	250	500	780	1806
10Co-n[c]	100	150	86	–	–	–	1332
16Co-a[a]	70	200	118	230	430	660	1626
16Co-b[b]			46	100	250	400	2190
16Co-c	45	100	67	150	250	450	2072
16Co-d[c]	100	150	122	250	600	800	1425
16Co-e[a]	67	165	105	233	450	700	1638
16Co-f	70	130	95	230	430	700	1607
16Co-g[b]			75	220	375	550	1776
16Co-h[c]	45	67	55	100	220	400	2278
16Co-i	30	75	47	90	200	300	2473
16Co-j[b]			70	130	300	450	2011
16Co-k	50	70	59	100	250	400	2277
16Co-l[a]	40	100	63	135	300	450	2008
16Co-m[c]	33	65	46	90	170	300	2411
16Co-n	100	133	115	250	550	800	1480

† See Fig. 3 for definition of symbols.
[a] Failure source: elliptical pore.
[b] Failure source: circular pore.
[c] Failure source: machining damage.

After the indenter contacts and penetrates the specimen, the plastically deformed area surrounding the impression is formed and this gives rise to surface tensile zones close to the contact zone [23]. The radial (Palmqvist) crack can be formed at the tip of the indentation impression upon unloading. On the other hand, penetration may cause a subsurface median (penny-like) crack immediately under the impression after indentation, eventually leading to a radial (half-penny-like) crack on unloading. Vickers indentation of brittle materials without any metallic phase is found to lead to the development of penny-shaped cracks under the indentation impression; these cracks break through the compressive surface layer upon continued loading and unloading, finally forming a radial–median crack. The size of crack that forms is proportional to $P^{2/3}$ ($c = kP^{2/3}$) [33–35].

Fig. 5 shows the average crack sizes (a and c) as a function of indentation loads. The lines exhibit a linear relationship for the Palmqvist crack length (a) and the radial–median crack length (c) plotted against indentation load (P), rather than proportional to $P^{2/3}$ for the radial–median crack. In addition, fracture surface analyses in Fig. 6 showed that fracture occurred from the median–radial crack shape just below the impression. This implies that the WC–Co fractures from radial–median cracks even if Palmqvist cracks form first. The inconsistent results using indentation

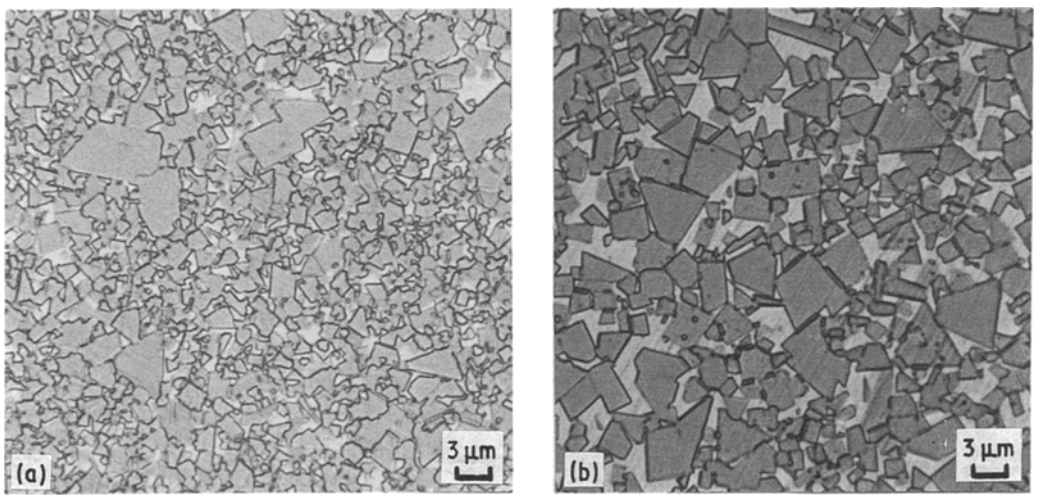

Figure 4 Polished, etched surfaces showing microstructures of (a) WC–10 wt % Co and (b) WC–16 wt % Co.

TABLE II Comparisons of mechanical properties of WC–Co

	WC–10 wt % Co	WC–16 wt % Co
Hardness (GPa)	13.8 ± 0.6	15.4 ± 1.2
Strength (MPa)	1930 ± 210	2020 ± 350
Fracture toughness ($MPa\,m^{1/2}$)		
Fracture surface analyses		
Flaw size, $C^*(ab)^{1/2}$ (Equation 3)	16.2 ± 1.2	19.9 ± 0.8
Mirror constant M_1 (Equation 4)	15.9 ± 1.0	18.7 ± 0.7
M_2	16.4 ± 0.7	19.7 ± 0.8
M_3	16.3 ± 0.8	19.9 ± 0.8
Indentation techniques	36.5 ± 0.8[a]	37.2 ± 3.7[a]
	17.7 ± 0.7[b]	20.7 ± 1.1[b]
	17.5 ± 1.3[c]	19.6 ± 1.0[c]
Literature values	13–17[d]	16–21[d]

[a] Fracture toughness (Equation 1) using Palmqvist crack length (a).
[b] Fracture toughness (Equation 1) using radial–median crack length (c)
[c] $K_C = 0.016(E/H)^{1/2}Pc^{-3/2}$ (Equation 2).
[d] Literature data (large crack model, [10, 14, 21]).

techniques strongly suggest that fracture toughness evaluation by the Palmqvist indentation crack model should be re-examined for use with WC–Co composites. The toughness values, however, calculated based on the radial–median crack model (Equation 2) agree

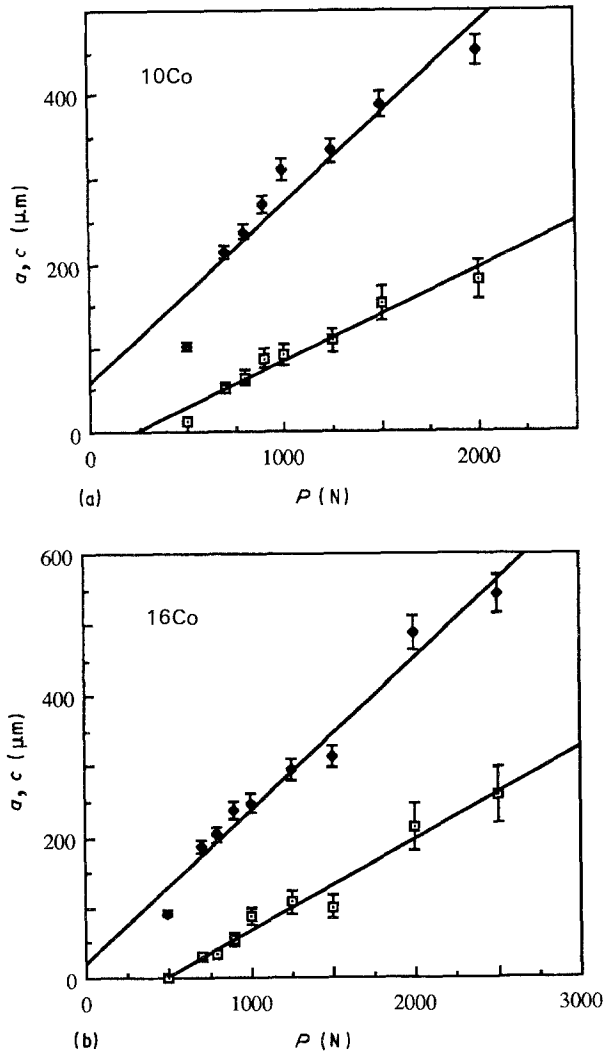

Figure 5 Relation between crack length a, c and indentation load P. □ a, ● c.

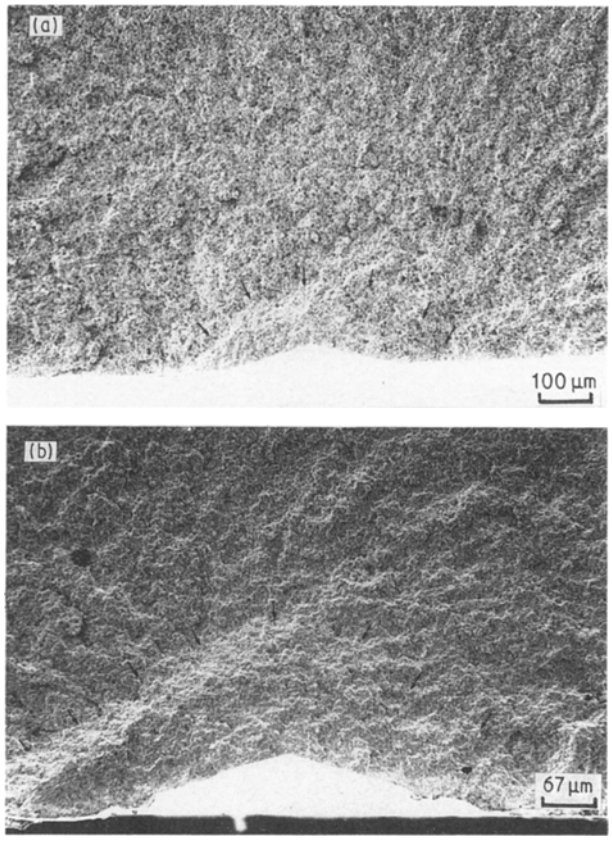

Figure 6 Observation of the fracture surface around an indentation impression exhibiting the crack of radial/median crack shape. (a): P = 800 N, WC–10 wt % Co; (b): P = 1500 N, WC–16 wt % Co.

well with those obtained in the literature [4, 10] using large crack techniques for similar WC–Co composites.

Fracture toughness by flaw size and mirror constants were summarized in Table II. Table III was obtained by measurement of crack sizes and surrounding topography on the fracture surfaces. Fracture toughness values obtained from fracture surface measurements (Equations 3 and 4) result in very consistent data with fracture toughness values calculated from Equation 2. More data are needed to assure the accuracy of the mirror and crack branching constants, but they are useful as estimates of the stress at fracture (Equations 4 and 5) for in-service failures of WC–Co

TABLE III Comparisons of R_i/C^*, mirror constants and branching stress intensity factors of WC–Co composites

	WC–10 wt % Co	WC–16 wt % Co
R_i/C^*[a]		
R_1/C^*	4–6	2–3
R_2/C^*	9–11	4–5
R_3/C^*	15–17	5–7
Mirror constant[b] ($MPa\,m^{1/2}$)		
M_1	27–31	23–26
M_2	40–43	32–36
M_3	50–55	42–45
Branching stress intensity factor[c] ($MPa\,m^{1/2}$)		
K_{B1}	34–38	28–33
K_{B2}	49–53	40–45
K_{B3}	62–68	51–56

[a] R_i/C^*, i = 1, 2, 3 and $C^* = (a^*b^*)^{1/2}$.
[b] $M_i = \sigma_m R_i^{1/2}$, i = 1, 2, 3
[c] $K_{Bi} = 1.24M_i$, i = 1, 2, 3.

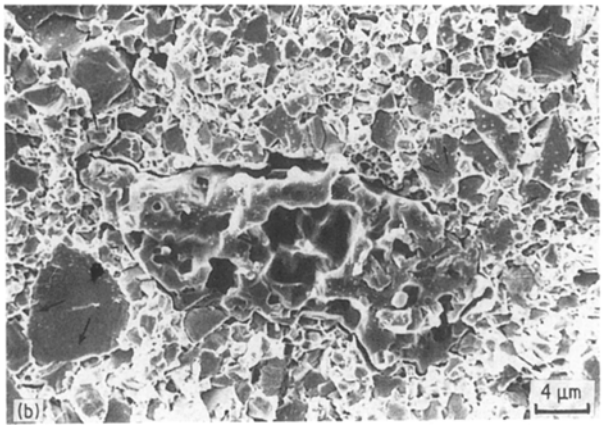

Figure 7 (a) Fracture surface and (b) failure-initiating source showing a non-uniformly dispersed cobalt phase at the origin of failure of WC–16 wt % Co.

components. This study demonstrates that fracture surface analysis developed for glasses and polycrystalline materials can also be applied to WC–Co composites.

SEM photos in Figs 7 and 8 show fracture surface features of 10 and 16 wt % Co composites. The arrows indicate the failure-initiating flaws. In Fig. 7b it is seen that an internal microstructural defect associated with a non-uniformly dispersed cobalt phase acted as the source of failure. A microprobe unit detected only high cobalt peaks at the failure origin. It has been suggested [36, 37] that the formation of cracks around microstructural defects such as agglomerates–aggregates is due to the density difference between the defects and the matrix. The defects have an important role on the density and set up residual stresses which reduce strength [36, 37]. Fig. 7b indicates that cracks nucleate at or around weakly linked regions and evidently act as stress concentrators. It is found that stress concentration and residual stress will be higher at the interface and can substantially reduce the load required to fracture materials [38, 39].

Careful examination of failure sources identify cracks from machining damage (Fig. 8a) resulting from a typical grinding operation or surface finishing. The flaw which is seen above the machining damage, acts similar to an indentation crack [40]. If a specimen with machining flaws is subjected to a tensile load, failure will ensue when the stress-intensity factor at the tips of these flaws becomes critical. The stress-intensity at the tips of these cracks will depend on their orientation to the load axis, the crack size, and the stress concentration effects at the bottom of the machining groove. These parameters will greatly influence the initiation of fracture [41, 42]. In addition to machining damage, single pores and/or pore clusters often have been found to be the failure-initiating source in many materials. Several studies [43–45] show that the size of pore is typically in the range of 10 to 200 μm depending on materials. The strength of the materials generally

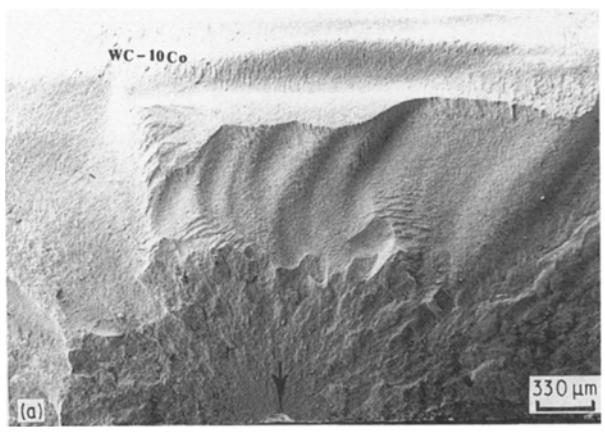

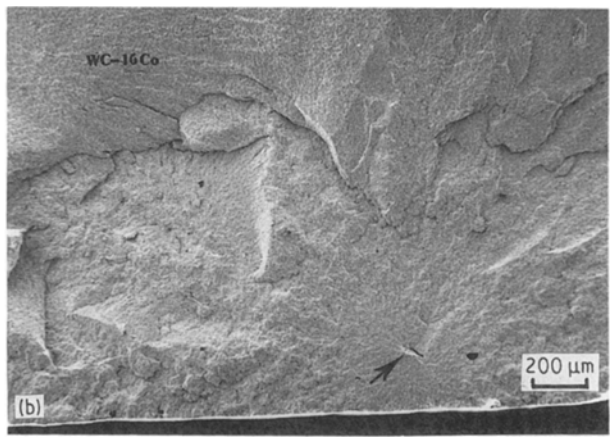

Figure 8 Fracture surface micrographs showing failure origins such as (a) machining damage and (b) pore.

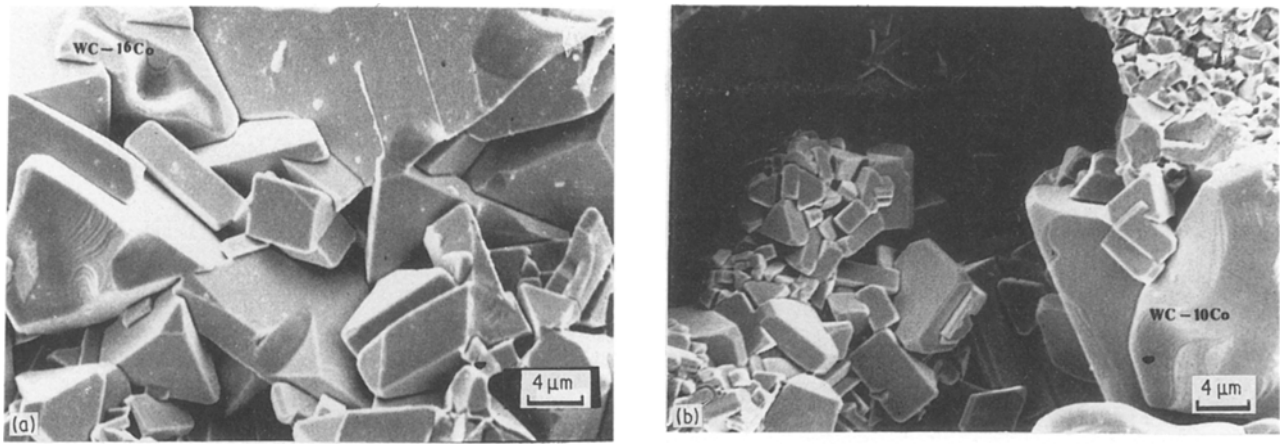

Figure 9 SEM photo showing the interior microstructure of a pore. Pores are major failure-initiating sources in WC–Co composites. (a) Notice the exaggerated grain growth and (b) notice that the grain boundaries without a cobalt phase are quite apparent inside the pore.

decreases with increasing pore size and its population. In this study, most WC–Co flexure bars failed due to pores (Fig. 8b) which most likely resulted from the cooling stage of sintering. It is known that pores in WC–Co composites are pipe-shaped and the shrinkage of metal (cobalt) generally results in about 1 or 2 vol % of porosity [46].

Fig. 9 shows the microstructure inside a pore in which exaggerated grain growth and no cobalt phase were found. In Fig. 10a (fracture surface above machining damage) fracture markings (river patterns) on transgranular faces of WC grains show local varied directions of crack propagation. Fig. 10b (fracture surface around the pore) shows the transgranular fracture for larger WC particles and intergranular fracture features for small WC particles. Fig. 10c shows another failure mode observed in WC–Co in which crack propagation is continued by connection of small pores. (Lines indicate the boundaries of pores.)

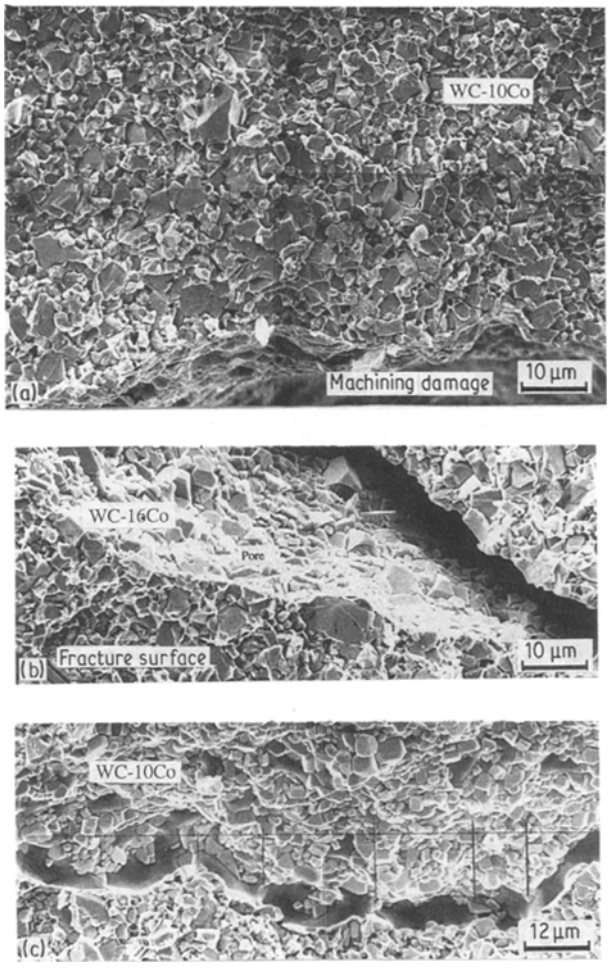

Figure 10 SEM photos showing crack propagation and fracture modes (a) above the machining damage, (b) around pores and (c) fails by pore connection.

5. Summary

Toughness measurement techniques based on the Palmqvist crack analysis need to be re-examined due to the disagreement of fracture toughness values obtained by different indentation methods. The indentation techniques of Lawn, Marshall and coworkers [18, 19] agree with the large crack techniques for these WC–Co composites. This paper suggests that fracture toughness evaluation by $W = P/4c$ where c is half the surface trace of an indentation crack measured from the centre, rather than $W = (P - P_0)/4a$, seems to be acceptable for higher indentation loads. More tests are needed, however, to determine the difference in fracture behaviour between the radial crack system and the Palmqvist crack system.

Fracture surfaces similar to those seen in glasses and ceramics are observed in WC–Co. The principles of fracture surface analysis that have been developed for other ceramics can be applied to WC–Co composites. Some cobalt bonded WC alloys fail due to machining damage, pores and excessive cobalt binder phase concentration. These failure sources indicate that the strength of WC–Co can be improved by changing processing variables such as sintering time or temperature.

References

1. F. OSTERSTOCK, Thesis, d'Etat, University of Caen, France (1980).
2. H. G. TATTERSALL and G. TAPPIN, *J. Mater. Sci.* **1** (1966) 296.
3. R. W. DAVIDGE and G. TAPPIN, *Proc. Brit. Ceram. Soc.* **15** (1970) 47.
4. J. L. CHERMANT and F. OSTERSTOCK, *J. Mater. Sci.* **11** (1976) 1939.
5. J. L. CHERMANT, A. DESCHANVRES and A. IOST, in "Fracture Mechanics of Ceramics", Vol. 1, edited by

R. C. Bradt, D. P. H. Hasselman and F. F. Lange (Plenum, New York, 1974).
6. P. KENNY, *Powder Metall.* **14** (1971) 22.
7. D. K. SHETTY, I. G. WRIGHT, P. N. MINCER and A. H. CLAUER, *J. Mater. Sci.* **20** (1985) 1873.
8. J. LANKFORD, *ibid.* **1** (1982) 493.
9. J. R. PICKENS and J. GURLAND, *J. Mater. Sci. Eng.* **33** (1978) 135.
10. J. HONG and P. SCHWARZKOPF, ASTM STP 855 (American Society for Testing and Materials, Philadelphia, 1984) p. 297.
11. R. C. LEUTH, PhD thesis, Michigan State University (1972).
12. S. S. YEN, Master Thesis, Lehigh University (1971).
13. R. C. LEUTH, *Fract. Mech. Ceramics* **2** (1974) 791.
14. E. A. ALMOND and B. ROEBUCK, *Met. Tech.* March (1978) 92.
15. Y. W. MAI, *J. Amer. Ceram. Soc.* **5**(1976) 491.
16. C. T. PETER, *J. Mater. Sci.* **14** (1979) 1619.
17. P. KENNY, *Powder Metall.* **14** (1971) 22.
18. G. R. ANSTIS, P. CHANTIKUL, B. R. LAWN and D. B. MARSHALL, *J. Amer. Ceram. Soc.* **64** (1981) 533.
19. P. CHANTIKUL, G. R. ANSTIS, B. R. LAWN and D. B. MARSHALL, *ibid.* **64** (1981) 539.
20. S. M. WIEDERHORN, S. W. FREIMAN, E. R. FULLER, Jr. and H. RICHER, ASTM STP 844 (American Society for Testing and Materials, Philadelphia, 1984) p. 95.
21. J. HONG and J. GURLAND, in "Science of Hard Materials", edited by R. K. Viswanadham, D. J. Rowcliffe and J. Gurland (Plenum, New York, 1983) p. 649.
22. J. M. OGILVY, C. M. PERROTT and J. W. SIUTER, *Wear* **43** (1977) 239.
23. C. M. PERROTT, *ibid.* **45** (1977) 293.
24. R. W. RICE, ASTM STP 829 (American Society for Testing and Materials, Philadelphia, 1984) p. 5.
25. J. J. MECHOLSKY and S. W. FREIMAN, ASTM STP 733 (American Society for Testing and Materials, Philadelphia, 1981) p. 246.
26. J. J. MECHOLSKY and S. W. FREIMAN, ASTM STP 678 (American Society for Testing and Materials, Philadelphia, 1980) p. 135.
27. J. J. MECHOLSKY, R. W. RICE and S. W. FREIMAN, *J. Amer. Ceram. Soc.* **57** (1974) 440.
28. H. P. KIRCHNER and J. C. CONWAY, Jr., *ibid.* **70** (1987) 565.
29. *Idem, ibid.* **70** (1987) 413.
30. *Idem, ibid.* **70** (1987) 419.
31. J. C. NEWMAN, Jr. and I. S. RAJU, NASA TP 1578 (1979).
32. K. RAVI-CHADAR and W. G. KNAUSS, *Int. J. Fract.* **26** (1984) 65.
33. B. R. LAWN and M. V. SWAIN, *J. Mater. Sci.* **10** (1975) 113.
34. B. R. LAWN and E. R. FULLER, *ibid.* **10** (1975) 2016.
35. M. T. LAUGIER, *Key Eng. Mater.* **32** (1989) 77.
36. F. F. LANGE, *J. Amer. Ceram. Soc.* **66** (1983) 396.
37. R. W. RICE, in "Processing of Crystalline Ceramics", edited by H. H. Palmour, R. F. Davis and T. M. Hare (Plenum, New York 1978) p. 303.
38. J. HEINRICH and D. MUNZ, *Amer. Ceram. Soc. Bull.* **59** (1980) 1221.
39. J. P. SINGH, *Adv. Ceram. Mater.* **3** (1988) 18.
40. R. W. RICE and J. J. MECHOLSKY, Jr., in "The Science of Ceramic Machining and Surface Finishing II", edited by B. J. Hockey and R. W. Rice, National Bureau of Standards Special Publication 562 (1979) p. 351.
41. D. C. CRAMER, R. E. TRESSLER and R. C. BRADT, *J. Amer. Ceram. Soc.* **60** (1977) 230.
42. R. E. TRESSLER, R. A. LANGESIEPEN and R. C. BRADT, *ibid.* **57** (1974) 226.
43. A. G. EVANS and R. W. DAVIDGE, *J. Mater. Sci.* **5** (1970) 314.
44. *Idem, J. Nucl. Mater.* **33** (1969) 249.
45. A. G. EVANS and G. TAPPIN, *Proc. Br. Ceram. Soc.* **20** (1972) 275.
46. R. J. NELSON and D. R. MILNER, *Powder Metall.* **15** (1972) 346.

Received 7 November
and accepted 12 December 1989